Commun. Comput. Phys.
doi: 10.4208/cicp.160110.290610a

Vol. **9**, No. 4, pp. 974-993
April 2011

# Numerical Simulations of Hydrodynamics of Nematic Liquid Crystals: Effects of Kinematic Transports

Shupeng Zhang[1], Chun Liu[2] and Hui Zhang[1,*]

[1] *School of Mathematical Sciences, Beijing Normal University, Beijing 100875, China.*
[2] *Department of Mathematics, Pennsylvania State University, University Park, PA 18601, USA.*

Received 16 January 2010; Accepted (in revised version) 29 June 2010

Communicated by Pingwen Zhang

Available online 2 November 2010

**Abstract.** In this paper, we investigate the effects of kinematic transports on the nematic liquid crystal system numerically and theoretically. The model we used is a "1+2" elastic continuum model simplified from the Ericksen-Leslie system. The numerical experiments are carried out by using a Legendre-Galerkin spectral method which can preserve the energy law in the discrete form. Based on this highly accurate numerical approach we find some interesting and important relationships between the kinematic transports and the characteristics of the flow. We make some analysis to explain these results. Several significant scaling properties are also verified by our simulations.

**AMS subject classifications**: 65M70, 76A15

**Key words**: Nematic liquid crystals, kinematic transports, Legendre-Galerkin spectral method, tumbling, flow-aligning.

## 1 Introduction

When the liquid crystals (LCs) are in nematic phase the molecules have long-range orientational order and can be easily aligned by external forces. This property results in many interesting and important phenomena, such as defects and textures. Many efforts have been made on theories describing the behavior of nematic LCs, for example, Onsager hard-rod model, Ericksen-Leslie (EL) theory, Maier-Saupe mean field theory, Q tensor theory, etc. Each model developed through a theory has its own merits in studying some aspects of nematic LCs.

*Corresponding author. *Email addresses:* shupeng.zhang@gmail.com (S. Zhang), liu@math.psu.edu (C. Liu), hzhang@bnu.edu.cn (H. Zhang)

 

The kinematic motions of the molecules is a fundamental topic in the study of nematic LCs. These motions can transform the alignment of molecules and further induce the change of physical properties of nematic LCs. Based on a kinetic model extended from Doi theory, Yu and Zhang studied the microstructure formation and defects dynamics arising in LC polymers in plane shear flow in [1]. Taken the long-range order elasticity into account Tsuji and Rey used a Q tensor theory to make an extensive analysis of the flow orientation modes of sheared liquid crystalline materials [2]. In [3] Feng et al. simulated the roll cells and disclinations in sheared nematic polymers. All these works were carried out with fixed tumbling parameter. Wang extended the Kuzuu and Doi theory to get a model with different configurations of molecules [4].

In EL theory a vector field **d** is used to depict the alignment of the molecules. The evolution of **d** expresses the kinematic motions. When the size of the molecules is small compared with the scale of the macroscopic fluid, **d** is just transported by the flow trajectory. When the size of the molecules are big enough, the effect of stretch by the fluid on **d** must be taken into account. This difference is reflected by the kinematic transport term of **d**. In the big molecule case, the parameter related to the shape of the molecules is important. In the original EL theory this parameter is called tumbling parameter. Effect of different tumbling parameter and Ericksen number on spatial development of director orientation in pressure-driven channel flow was investigated by Chono et al. in [5].

Lin and Liu et al. simplified the EL system [6–9] and they used a penalty function to relax the nonlinear constraint. Based on this simplified elastic continuum theory, many numerical experiments have been carried out to study the kinematic behaviors of nematic LCs. For small molecule cases, in [10] Liu and Walkington used a $C^1$ finite element to make sure that the test function is in the right space and the energy law is kept in discrete form. A mixed finite element was applied in [11] to avoid the construction of the complicated $C^1$ element. But the mixed method introduces new variables and increase the complication of implementation. In [12] Lin and Liu proposed a simpler $C^0$ finite element method to improve the efficiency of the numerical simulations. Spectral method for the system on rectangle domains with periodic boundary conditions was studied in [13] by Du et al.. For big molecule cases, a numerical scheme was proposed in [8] in order to preserve the energy law. In [9] an efficient and accurate spectral method was carried out on an axi-symmetric domain and dynamics of defect motions was studied. The numerical simulations reveal the significant impact of molecule shape on the moving speed of defects. Finite difference scheme in "1+2" dimension case was designed in [14]. They observed many valuable tumbling phenomena using the energy law preserving scheme.

In this paper, high order spectral method is used to simulate the "1+2" model. This model is similar to that in [14]. Instead of observations of tumbling phenomena therein, we mainly focus on the effect of kinematic transports on the nematic LC system. The kinematic transport is mainly determined by the shape of molecules and shear rate. We want to show that even with this simple model, several flow modes can be predicted and some significant scaling properties can be verified. Meanwhile, we want to reveal the relationship between two important parameters and the flow behavior. Since the nonlin-

ear constraint is relaxed by a penalty function, the spectral method which is usually used for smooth functions is suitable for the simulations. Furthermore, we can use Galerkin method to design a numerical scheme which satisfies the discrete energy law. The preservation of discrete energy law can enhance the stability of system, especially when defects are involved. Through the numerical results, we can find or verify some interesting and important relationships between the kinematic transports and the characteristics of the flow. We compare our results with those of other models. This paper is organized as follows. We first introduce the model in Section 2. In the third section, we present the numerical method. Numerical results and discussions are given in Section 4. Finally, we have some conclusions and remarks.

## 2 Model

In this section, we introduce the elastic continuum model used in our simulations.

### 2.1 Governing equations

The original hydrodynamic theory of nematic LCs established by Ericksen and Leslie [15, 16] covers the conservation of mass, linear momentum and angular momentum. We start from the following simplified model by Lin and Liu [6,7]:

$$\mathbf{u}_t+(\mathbf{u}\cdot\nabla)\mathbf{u}+\nabla p-\mu\Delta\mathbf{u}-\lambda\nabla\cdot\sigma=0, \tag{2.1a}$$

$$\nabla\cdot\mathbf{u}=0, \tag{2.1b}$$

$$\sigma=(\nabla\mathbf{d})^T\nabla\mathbf{d}, \tag{2.1c}$$

$$\mathbf{d}_t+(\mathbf{u}\cdot\nabla)\mathbf{d}=\gamma(\Delta\mathbf{d}-\mathbf{f}(\mathbf{d})). \tag{2.1d}$$

Here, $\mathbf{u}$ represents the velocity of the nematic LC fluid, $p$ is the pressure, $\mathbf{d}$ is the orientation of the molecules, $\mathbf{u},\mathbf{d}:\Omega\times\mathbb{R}^+\to\mathbb{R}^n$, $p:\Omega\times\mathbb{R}^+\to\mathbb{R}$ and $\Omega\subset\mathbb{R}^n$, $\mathbf{x}\in\Omega$ is the Eulerian coordinate. $\mu,\lambda,\gamma$ are positive constants. $\mathbf{f}(\mathbf{d})=(4/\epsilon^2)(|\mathbf{d}|^2-1)\mathbf{d}$ can be seen as a penalty function to approximate the constraint $|\mathbf{d}|=1$ which is due to the molecules being of similar size. The corresponding energy density is $F(\mathbf{d})=(1/\epsilon^2)(|\mathbf{d}|^2-1)^2$. Notice that the transportation term of $\mathbf{d}$ here is $\frac{D}{Dt}\mathbf{d}=\mathbf{d}_t+(\mathbf{u}\cdot\nabla)\mathbf{d}$, which means that $\mathbf{d}$ is just transported by the flow trajectory. This is due to the fact that the size of the molecules is small and the directors are not affected by the stretching of the fluid.

For the big molecule case, the hydrodynamical system of nematic LCs becomes [8,9]:

$$\mathbf{u}_t+(\mathbf{u}\cdot\nabla)\mathbf{u}+\nabla p-\mu\Delta\mathbf{u}-\lambda\nabla\cdot\sigma=0, \tag{2.2a}$$

$$\nabla\cdot\mathbf{u}=0, \tag{2.2b}$$

$$\sigma=(\nabla\mathbf{d})^T\nabla\mathbf{d}+\beta(\Delta\mathbf{d}-\mathbf{f}(\mathbf{d}))\mathbf{d}^T+(\beta+1)\mathbf{d}(\Delta\mathbf{d}-\mathbf{f}(\mathbf{d}))^T, \tag{2.2c}$$

$$\mathbf{d}_t+(\mathbf{u}\cdot\nabla)\mathbf{d}+D_\beta(\mathbf{u})\mathbf{d}=\gamma(\Delta\mathbf{d}-\mathbf{f}(\mathbf{d})), \tag{2.2d}$$

where

$$D_\beta(\mathbf{u}) = \beta\nabla\mathbf{u} + (1+\beta)(\nabla\mathbf{u})^T, \quad \text{for } \beta \in \mathbb{R}.$$

Here the kinematic transports of $\mathbf{d}$ are

$$\frac{D}{Dt}\mathbf{d} = \mathbf{d}_t + (\mathbf{u}\cdot\nabla)\mathbf{d} + D_\beta(\mathbf{u})\mathbf{d}.$$

The extra term $D_\beta(\mathbf{u})$ comes from the stretching of the fluid and the parameter $\beta$ depends on the shape of the molecules [8,9]. Notice that $D_\beta(\mathbf{u})$ can be rewritten as

$$D_\beta(\mathbf{u}) = -\frac{\nabla\mathbf{u} - (\nabla\mathbf{u})^T}{2} - (-2\beta-1)\frac{(\nabla\mathbf{u})^T + \nabla\mathbf{u}}{2}.$$

The parameter $-2\beta-1$ is called the *reactive parameter*, or *tumbling parameter* in EL theory [17]. For nematic LCs composed of rod-like molecules we have $\beta < -0.5$ while for those composed of disc-like molecules $\beta > -0.5$. In [8,9] $\beta$ is confined within the interval $[-1,0]$. Actually $\beta$ can take any real value and when $|2\beta+1| < 1$ the nematic LC is *tumbling* while when $|2\beta+1| > 1$ it is *flow-aligning*. This is due to the fact that $\beta$ also depends on the second and fourth moments of the distribution of molecules about the nematic director [18] and this dependence can not be predicted by EL theory itself. When the nematic LC is flow-aligning it has steady state in a simple shear flow and there will be a flow-aligning angle related to $\beta$. We will study all these cases in our simulations.

We want to point out that once we have the internal elastic energy

$$W(\mathbf{d}) = \frac{\lambda}{2}\|\nabla\mathbf{d}\|_{L^2}^2 + \lambda\int_\Omega F(\mathbf{d})\mathrm{dx}$$

and the kinematic transports of $\mathbf{d}$, we can use the least action principle, or equivalently the principle of virtual work to derive the induced stress term $\sigma$. The derivation with the least action principle uses the variation with respect to domain. We refer to [19] for the details. We can see from the expression of $\sigma$ that this induced stress term depends on the parameter $\beta$. $\sigma$ and the kinematic transport of $\mathbf{d}$ are acting force and reacting force between the flow and the molecules. Different kinematic transports give different induced stresses and the dependency is reflected by $\beta$.

## 2.2 Boundary conditions

In order to investigate the behaviors of nematic LCs under shear flow, the boundary condition (B.C.) of $\mathbf{u}$ is chosen as:

$$\mathbf{u}\cdot\mathbf{n} = 0, \quad \frac{\partial(\mathbf{u}\cdot\tau)}{\partial\mathbf{n}} = \mathbf{g}_\mathbf{u}\cdot\tau, \quad \text{on } \partial\Omega, \tag{2.3}$$

where $\mathbf{n}$ denotes the outer normal vector on the boundary and $\tau$ is the tangential component to $\partial\Omega$. This B.C. is used in our simulations to approximate the B.C. of the plane Couette flow.

Instead of strong anchoring B.C. which fixes $\mathbf{d}$ on the boundary, we apply the following Robin B.C.:

$$\frac{\partial \mathbf{d}}{\partial \mathbf{n}} = -\frac{2}{\delta}(\mathbf{d}-\mathbf{d}^0), \quad \text{on } \partial\Omega, \tag{2.4}$$

where $\delta>0$. Actually under this choice of B.C., one term called anchoring energy is added into the total energy. The parameter $\delta$ reflects the strength of the anchoring. We believe that this is more reasonable than fixing $\mathbf{d}$ on the boundary.

**Remark 2.1.** Similar B.C.s for nematic LCs which are called free-slip B.C.s have been studied analytically by Liu and Shen in [20]. The choice of B.C.s here has another significance. When we use Galerkin method to approach the system, the solutions and the test functions can be in the same space. This property of consistence makes the derivation of energy law from weak form feasible, even when the B.C.s are nonhomogeneous.

### 2.3 Energy law

The system possesses the following energy law:

$$\begin{aligned}
&\frac{\mathrm{d}}{\mathrm{d}t}\Big(\frac{1}{2}\|\mathbf{u}\|_{L^2}^2+\frac{\lambda}{2}\|\nabla\mathbf{d}\|_{L^2}^2+\lambda\int_\Omega F(\mathbf{d})\mathrm{dx}+\frac{\lambda}{\delta}\int_{\partial\Omega}|\mathbf{d}-\mathbf{d}_0|^2\mathrm{dS}\Big)\\
=&-\Big(\mu\|\nabla\mathbf{u}\|_{L^2}^2+\frac{\lambda}{\gamma}\|\mathbf{d}_t+(\mathbf{u}\cdot\nabla\mathbf{d})\mathbf{d}+D_\beta(\mathbf{u})\mathbf{d}\|_{L^2}^2\Big)\\
&+\int_{\partial\Omega}(\mathbf{g_u}\cdot\mathbf{u})\mathrm{dS}+\int_{\partial\Omega}(\sigma_1:\mathbf{u}\otimes\mathbf{n})\mathrm{dS},
\end{aligned} \tag{2.5}$$

where

$$\sigma_1=\beta(\Delta\mathbf{d}-\mathbf{f}(\mathbf{d}))\mathbf{d}^T+(\beta+1)\mathbf{d}(\Delta\mathbf{d}-\mathbf{f}(\mathbf{d}))^T.$$

The derivation is straightforward: add (2.2a) multiplied by $\mathbf{u}$ to (2.2d) multiplied by $\lambda/\gamma(\mathbf{d}_t+\mathbf{u}\cdot\nabla\mathbf{d}+D_\beta(\mathbf{u})\mathbf{d})$, and then integrate on $\Omega$, reform the terms by integration by parts if necessary. The energy law plays an important role in both theoretical [6, 7] and numerical analysis, especially when the physical singularities are involved. It is worth noticing that the nonhomogeneous B.C.s arouse some external forces acting on the system, which may break the decay of energy.

**Remark 2.2.** If we replace the B.C. of $\mathbf{u}$ with the non-slip B.C. and replace $\mathbf{d}_t+(\mathbf{u}\cdot\nabla\mathbf{d})\mathbf{d}+D_\beta(\mathbf{u})\mathbf{d}$ with $-\gamma\frac{\delta W}{\delta\mathbf{d}}$, the energy law is then independent on the kinematic transports of $\mathbf{d}$. This is due to the fact that the forces between the fluid and the molecules are internal.

### 2.4 "1+2" model

The so-called "1+2" dimension model preserves many properties of the full system. We will use this model in our simulations. Assume that

$$\mathbf{u}=(0,v(z),0), \quad p=p(z), \quad \mathbf{d}=(0,d_2(z),d_3(z)), \quad z\in[-1,1],$$

then we have:

$$v_t = \mu v_{zz} + \lambda \tau_z, \tag{2.6a}$$
$$\tau = \beta(d_{2zz} - f_2)d_3 + (\beta+1)(d_{3zz} - f_3)d_2, \tag{2.6b}$$
$$d_{2t} + \beta v_z d_3 = \gamma(d_{2zz} - f_2), \tag{2.6c}$$
$$d_{3t} + (\beta+1)v_z d_2 = \gamma(d_{3zz} - f_3). \tag{2.6d}$$

Let $\zeta$ be the shear rate, then the B.C.s are taken as:

$$v_z(-1) = \zeta, \qquad v_z(1) = \zeta, \tag{2.7a}$$
$$d_{2z}(-1) = \frac{2}{\delta}(d_2(-1) - d_2^0(-1)), \qquad d_{2z}(1) = -\frac{2}{\delta}(d_2(1) - d_2^0(1)), \tag{2.7b}$$
$$d_{3z}(-1) = \frac{2}{\delta}(d_3(-1) - d_3^0(-1)), \qquad d_{3z}(1) = -\frac{2}{\delta}(d_3(1) - d_3^0(1)). \tag{2.7c}$$

The parameters included in this system are $\mu,\lambda,\gamma,\epsilon$ and $\beta,\zeta$. We mainly focus on the impact of $\beta$ and $\zeta$ in this chapter.

## 3 Numerical method

The system (2.6a)-(2.7c) is solved by using a Legendre-Galerkin spectral method. In [14] Zhang and Bai solved a similar system with a finite difference method preserving the discrete energy law. As we will see in Section 4, the system with high shearing includes many rotations in space and fast tumbling in time and thus we prefer the high order spectral method. Fortunately, the discrete energy law can also be preserved based on our choice of B.C.s and numerical method. The details for the realizations of general Legendre-Galerkin spectral method can be found in [21]. We just present some key points of our scheme here.

For the time discretization we adopt the Crank-Nicolson scheme:

$$\begin{cases} \dfrac{v^{n+1}-v^n}{dt} - \mu(v^{n+\frac{1}{2}})_{zz} - \dfrac{\lambda}{\gamma}(\tau^{n+\frac{1}{2}})_z = 0, \\ \dfrac{d_2^{n+1}-d_2^n}{dt} + \beta v_z^{n+\frac{1}{2}} d_3^{n+\frac{1}{2}} = \gamma\Big((d_2^{n+\frac{1}{2}})_{zz} - g_2^{n+\frac{1}{2}}\Big), \\ \dfrac{d_3^{n+1}-d_3^n}{dt} + (\beta+1)v_z^{n+\frac{1}{2}} d_2^{n+\frac{1}{2}} = \gamma\Big((d_3^{n+\frac{1}{2}})_{zz} - g_3^{n+\frac{1}{2}}\Big), \\ \tau^{n+\frac{1}{2}} = \Big(\dfrac{d_2^{n+1}-d_2^n}{dt} + \beta v_z^{n+\frac{1}{2}} d_3^{n+\frac{1}{2}}\Big)\beta d_3^{n+\frac{1}{2}} + \Big(\dfrac{d_3^{n+1}-d_3^n}{dt} + (\beta+1)v_z^{n+\frac{1}{2}} d_2^{n+\frac{1}{2}}\Big)(\beta+1)d_2^{n+\frac{1}{2}}, \end{cases}$$

where

$$v^{n+\frac{1}{2}} = \frac{v^{n+1}+v^n}{2}, \quad d_2^{n+\frac{1}{2}} = \frac{d_2^{n+1}+d_2^n}{2}, \quad d_3^{n+\frac{1}{2}} = \frac{d_3^{n+1}+d_3^n}{2},$$

and [8]

$$g_2^{n+\frac{1}{2}}=\frac{1}{\epsilon^2}[(d_2^{n+1})^2+(d_3^{n+1})^2+(d_2^n)^2+(d_3^n)^2-2](d_2^{n+1}+d_2^n),$$
$$g_3^{n+\frac{1}{2}}=\frac{1}{\epsilon^2}[(d_2^{n+1})^2+(d_3^{n+1})^2+(d_2^n)^2+(d_3^n)^2-2](d_3^{n+1}+d_3^n),$$

with initial data $\{v^0,d_2^0,d_3^0\}$ and B.C.s:

$$v_z^{n+\frac{1}{2}}(-1)=\zeta, \qquad v_z^{n+\frac{1}{2}}(1)=\zeta,$$
$$\delta d_{2z}^{n+\frac{1}{2}}(-1)=-2(d_2^{n+\frac{1}{2}}(-1)+d_2^0(-1)), \qquad \delta d_{2z}^{n+\frac{1}{2}}(1)=-2(d_2^{n+\frac{1}{2}}(1)+d_2^0(1)),$$
$$\delta d_{3z}^{n+\frac{1}{2}}(-1)=-2(d_3^{n+\frac{1}{2}}(-1)+d_3^0(-1)), \qquad \delta d_{3z}^{n+\frac{1}{2}}(1)=-2(d_3^{n+\frac{1}{2}}(1)+d_3^0(1)).$$

Notice that we have replaced $\gamma(\Delta\mathbf{d}-\mathbf{f}(\mathbf{d}))$ with $\mathbf{d}_t+(\mathbf{u}\cdot\nabla)\mathbf{d}+D_\beta(\mathbf{u})\mathbf{d}$ in the stress term to reduce the order of derivatives as in [8,12]. In [8,12] this replacement is used to implement a $C^0$ finite element method. Although the high order terms are easier to deal with by spectral method, we still do the replacement to reduce the loss of accuracy which is caused by the high order derivatives.

Let $P_n$ be the set of polynomials of degree not exceeding $n$ where $n\in\mathbb{N}$. The Legendre spectral-Galerkin method is to find $v^n$, $d_2^n$, $d_3^n\in P_N(n=1,2,3,\cdots,)$ such that for any $p$, $q$, $r\in P_N$,

$$\begin{cases}
\Big(\frac{v^{n+1}-v^n}{dt},p\Big)+\mu\Big(v_z^{n+\frac{1}{2}},p_z\Big)+\Big(\frac{\lambda}{\gamma}\tau^{n+\frac{1}{2}},p_z\Big)=\big(\mu v_z p+\frac{\lambda}{\gamma}\tau^{n+\frac{1}{2}}p\big)\big|_{-1}^1,\\
\Big(\frac{d_2^{n+1}-d_2^n}{dt}+\beta(v_z^{n+\frac{1}{2}}d_3^{n+\frac{1}{2}})+\gamma g_2^{n+\frac{1}{2}},q\Big)+\gamma\Big(d_{2z}^{n+\frac{1}{2}},q_z\Big)\\
\qquad\qquad=\sum_{z=-1,1}\Big(-\frac{2\gamma}{\delta}(d_2^{n+\frac{1}{2}}(z)-d_2^0(z))q(z)\Big),\\
\Big(\frac{d_3^{n+1}-d_3^n}{dt}+(\beta+1)(v_z^{n+\frac{1}{2}}d_2^{n+\frac{1}{2}})+\gamma g_3^{n+\frac{1}{2}},r\Big)+\gamma\Big(d_{3z}^{n+\frac{1}{2}},r_z\Big)\\
\qquad\qquad=\sum_{z=-1,1}\Big(-\frac{2\gamma}{\delta}(d_3^{n+\frac{1}{2}}(z)-d_3^0(z))r(z)\Big),\\
\tau^{n+\frac{1}{2}}=\Big(\frac{d_2^{n+1}-d_2^n}{dt}+\beta v_z^{n+\frac{1}{2}}d_3^{n+\frac{1}{2}}\Big)\beta d_3^{n+\frac{1}{2}}+\Big(\frac{d_3^{n+1}-d_3^n}{dt}+(\beta+1)v_z^{n+\frac{1}{2}}d_2^{n+\frac{1}{2}}\Big)(\beta+1)d_2^{n+\frac{1}{2}}.
\end{cases}$$

Actually we take the Legendre polynomials of degree not exceeding $N$ to be the basis functions of $P_N$. This is mainly because the inner product in Legendre spectral method is exactly the usual $L^2$ inner product and the discrete energy law can be derived from the weak form.

Let

$$E^n=\frac{1}{2}\|v^n\|_{L^2}^2+\frac{\lambda}{2}(\|d_{2z}^n\|_{L^2}^2+\|d_{3z}^n\|_{L^2}^2)+\lambda\int_{-1}^1 F(d_2^n,d_3^n)\mathrm{dx}$$
$$+\frac{\lambda}{\delta}\Big(\sum_{i=2,3}\Big(\sum_{x_j=-1,1}(d_i^n(x_j)+d_i^0(x_j))^2\Big)\Big),$$

since $v^n, d_2^n, d_3^n, p, q, r$ are in the same space $P_N$, we can take

$$p = v^{n+1} + v^n, \quad q = \frac{d_2^{n+1} - d_2^n}{dt}, \quad r = \frac{d_3^{n+1} - d_3^n}{dt}$$

to find the following energy law based on the above weak form,

$$\begin{aligned}\frac{E^{n+1}-E^n}{dt} = &-\frac{\lambda}{\gamma}\Big(\Big\|\frac{d_2^{n+1}-d_2^n}{dt} + \beta(v_z^{n+\frac{1}{2}} d_3^{n+\frac{1}{2}})\Big\|_{L^2}^2 + \Big\|\frac{d_3^{n+1}-d_3^n}{dt} + (\beta+1)(v_z^{n+\frac{1}{2}} d_2^{n+\frac{1}{2}})\Big\|_{L^2}^2\Big)\\ &-\mu\|v_z^{n+\frac{1}{2}}\|_{L^2}^2 + \Big(\mu v_z v^{n+\frac{1}{2}} + \frac{\lambda}{\gamma}\tau^{n+\frac{1}{2}} v^{n+\frac{1}{2}}\Big)\Big|_{-1}^{1} \triangleq El_r^{n+\frac{1}{2}}.\end{aligned}$$

The above system is still nonlinear. We are going to use the following fixed point iteration method:

$$\begin{cases}
\Big(\frac{v^s - v^n}{dt}, p\Big) + \mu\Big(\Big(\frac{v^s+v^n}{2}\Big)_z, p_z\Big) + \Big(\frac{\lambda}{\gamma}\tau^{s-\frac{1}{2}}, p_z\Big) = \Big(\mu v_z p + \frac{\lambda}{\gamma}\tau^{s-\frac{1}{2}} p\Big)\Big|_{-1}^{1},\\
\Big(\frac{d_2^s - d_2^n}{dt} + \beta(v_z^{s-\frac{1}{2}} d_3^{s-\frac{1}{2}}) + \gamma g_2^{s-\frac{1}{2}}, q\Big) + \gamma\Big(\Big(\frac{d_2^s+d_2^n}{2}\Big)_z, q_z\Big)\\
\qquad = \sum_{z=-1,1}\Big(-\frac{\gamma}{\delta}\Big(\frac{d_2^s(z)+d_2^n(z)}{2} - d_2^0(z)\Big) q(z)\Big),\\
\Big(\frac{d_3^s - d_3^n}{dt} + (\beta+1)(v_z^{s-\frac{1}{2}} d_2^{s-\frac{1}{2}}) + \gamma g_3^{s-\frac{1}{2}}, r\Big) + \gamma\Big(\Big(\frac{d_3^s+d_3^n}{2}\Big)_z, r_z\Big)\\
\qquad = \sum_{z=-1,1}\Big(-\frac{\gamma}{\delta}\Big(\frac{d_2^s(z)+d_2^n(z)}{2} - d_3^0(z)\Big) r(z)\Big),\\
\tau^{s-\frac{1}{2}} = \Big(\frac{d_2^s - d_2^n}{dt} + \beta v_z^{s-\frac{1}{2}} d_3^{s-\frac{1}{2}}\Big)\beta d_3^{s-\frac{1}{2}} + \Big(\frac{d_3^s - d_3^n}{dt} + (\beta+1) v_z^{s-\frac{1}{2}} d_2^{s-\frac{1}{2}}\Big)(\beta+1) d_2^{s-\frac{1}{2}},\\
v^{s-\frac{1}{2}} = \frac{v^{s-1}+v^n}{2}, \quad d_2^{s-\frac{1}{2}} = \frac{d_2^{s-1}+d_2^n}{2}, \quad d_3^{s-\frac{1}{2}} = \frac{d_3^{s-1}+d_3^n}{2}.
\end{cases}$$

We take $\{v^n, d_2^n, d_3^n\}$ as the starting point inside one time-step and set $v^{n+1} = v^s$, $d_2^{n+1} = d_2^s$, $d_3^{n+1} = d_3^s$ when

$$\|v^s - v^{s-1}\| + \|d_2^s - d_2^{s-1}\| + \|d_3^s - d_3^{s-1}\| < tol.$$

The convergence of the fixed point iteration method is discussed numerically in Section 4.

Notice that all the inner products in the iteration system are integrations of polynomials no more than $4N$ degree. They are evaluated by Legendre-Gauss-Lobatto (LGL) quadrature. For integrations of polynomials of degree not exceeding $2N-1$ the quadrature with $N+1$ LGL points are accurate. For polynomials of degree larger than $2N-1$ we need the quadrature with $2N+1$ LGL nodes. Fortunately we can always calculate the values of $u(x) \in P_N$ on the nodes of LGL quadrature with $2N+1$ points. This is actually an interpolation from the coarse grid to fine grid and the interpolation can be accurate for polynomials.

# 4 Numerical results and discussion

All the simulations are carried out with MATLAB and the results are visualized also by MATLAB.

## 4.1 Parameters

We seek the solutions in the polynomial space $P_{128}$, i.e., the number of the LGL nodes are 129. Tests with more nodes are also carried out and the results are almost the same. We just give the results with 129 nodes. $dt$ is chosen to be $1\times10^{-4}$. In all of our simulations this choice of $dt$ can make sure the fixed point iteration method work. The main parameters in the system are $\beta,\zeta,\gamma,\lambda,\mu,\delta$ and $\epsilon$. We mainly focus on the impact of $\beta$ and $\zeta$ and thus unless otherwise specified the other parameters are set to be: $\gamma=1,\lambda=1,\mu=1,\epsilon=3\times10^{-2},\delta=5\times10^{-5}$. We want to point out that $\epsilon$ is usually set to be about twice of the mesh size. Finally we set the tolerance of the fixed point iteration to be $1\times10^{-12}$.

## 4.2 Tests of numerical scheme

We give a benchmark example first and illustrate how we express our results. Take $\zeta=40,\beta=-0.6$ and the initial values to be

$$v^0(z)=\zeta z,\quad d_2^0(z)=-1,\quad d_3^0(z)=0,\quad z\in[-1,1].$$

The numerical result is depicted in Fig. 1.

The system goes to steady state finally. We can see the alignment of the molecules in steady state in Fig. 1.

From the energy plotting we can see that the energy does not decay at the beginning. This is due to nonhomogeneous B.C.s, or in other words, the action of external forces on

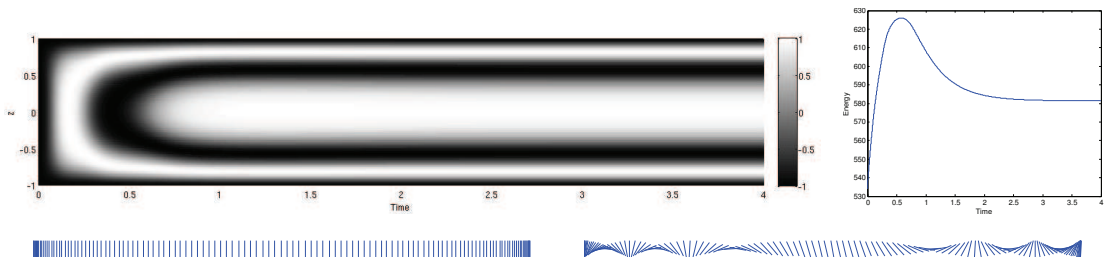


Figure 1: Top-left: Evolution of the $\mathbf{d}$. Gray colors represent $d_2$, i.e., the cosine value of the director angle. Top-right: Total energy plotting with respect to time. Lower-left: The initial molecule alignment along $z$-axis. Lower-right: The molecule alignment at t=4 when the solution is almost at steady state.

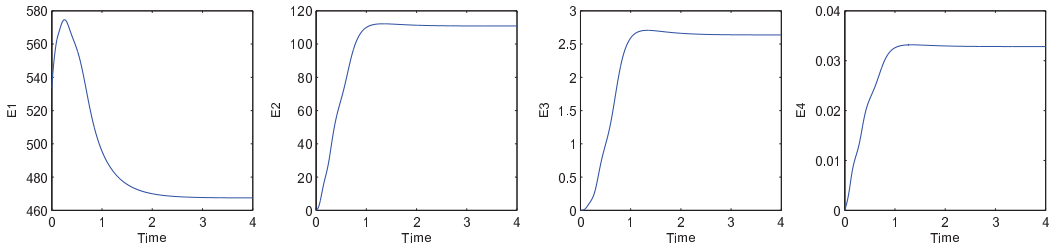


Figure 2: Plotting of kinetic energy $E_1$, elastic energy $E_2$ and $E_3$, surface energy $E_4$.

the system. Let $E=E_1+E_2+E_3+E_4$, where

$$E_1=\frac{1}{2}\|v\|_{L^2}^2, \qquad E_2=\frac{\lambda}{2}(\|d_{2z}\|_{L^2}^2+\|d_{3z}\|_{L^2}^2),$$
$$E_3=\lambda\int_{-1}^{1}F(d_2,d_3)\mathrm{d}x, \qquad E_4=\frac{\lambda}{\delta}\left(\sum_{i=2,3}\left(\sum_{x_j=-1,1}(d_i(x_j)-d_i^0(x_j))^2\right)\right).$$

The changes of these parts of total energy are depicted in Fig. 2. It can be seen from the plottings that the main competition is between $E_1$ and $E_2$ in this example.

The scheme we use satisfies the discrete energy law. Set

$$El^{n+\frac{1}{2}}=\left|\frac{E^{n+1}-E^n}{dt}-El_r^{n+\frac{1}{2}}\right|.$$

We check the discrete energy law in this example and depict $El^{n+1/2}$ in Fig. 3. It can be seen that $El^{n+1/2}<1.2\times10^{-7}$ all the time. This error arises from other factors, e.g., rounding error, other than numerical scheme. The discrete energy law insures the stability of time revolution.

Now we turn to the convergence of the fixed point iteration. At the beginning of the simulation it takes about 21 steps to converge inside one time-step. Denote the number of steps inside the first time step as $I_n$. The dependence of $I_n$ on $\beta$ is depicted in Fig. 4. The relationship between $I_n$ and $\beta$ given by linear fitness (polyfit) in MATLAB on $-0.1\leq\beta\leq0$ is

$$I_n\approx\frac{16.608}{0.019824-2\ln(\beta+1)}.$$

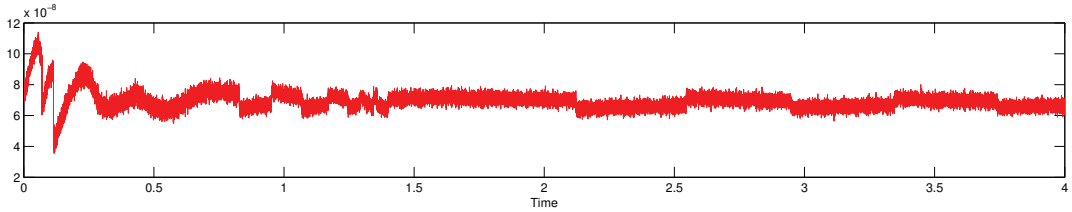


Figure 3: Discrete energy law.

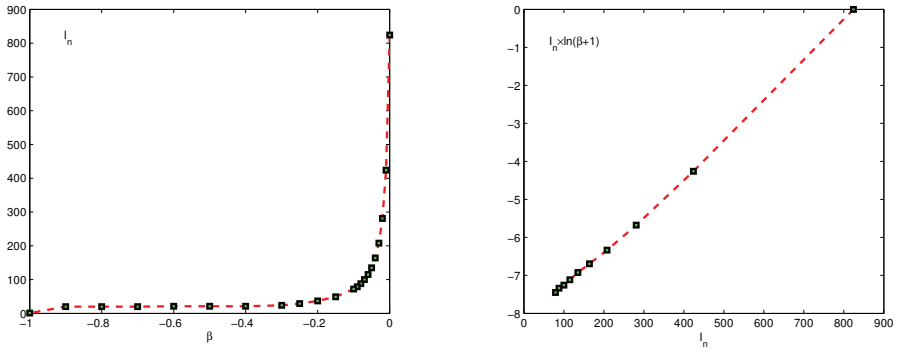


Figure 4: Dependence of $I_n$ on $\beta$.

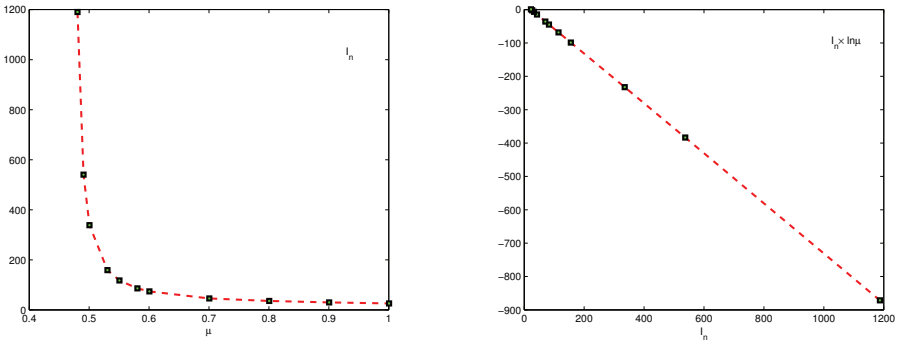


Figure 5: Dependence of $I_n$ on $\mu$.

We also consider the dependence of $I_n$ on the shear rate $\zeta$ when we fix $\beta=-0.3$. The tests reveal that $I_n$ increases with increased $\zeta$ but does not exceed 50 when $\zeta<3000$.

The dependence of $I_n$ on $\mu$ when $\beta=-0.3$ is given in Fig. 5 and the relationship by linear fitness in MATLAB is

$$I_n \approx \frac{17.73}{0.7483+\ln(\mu)}.$$

Since $\ln(1+(-0.3))=-0.3568\approx -0.7483/2$ we can guess that

$$I_n \approx \frac{17.73}{\ln(\mu)-2\ln(1+\beta)}.$$

This relationship can be proved by other tests. It tells us that $\mu>(1+\beta)^2$ should be guaranteed for the convergence of the fixed point iterations. This criterion is useful when $|1+\beta|$ is large, i.e., for the simulations of flow-aligning nematic LCs.

**Remark 4.1.** The criteria $\mu>(1+\beta)^2$ is partly determined by the choice of the numerical scheme. It is not necessary if you can solve the nonlinear system directly instead of fixed point iteration method.

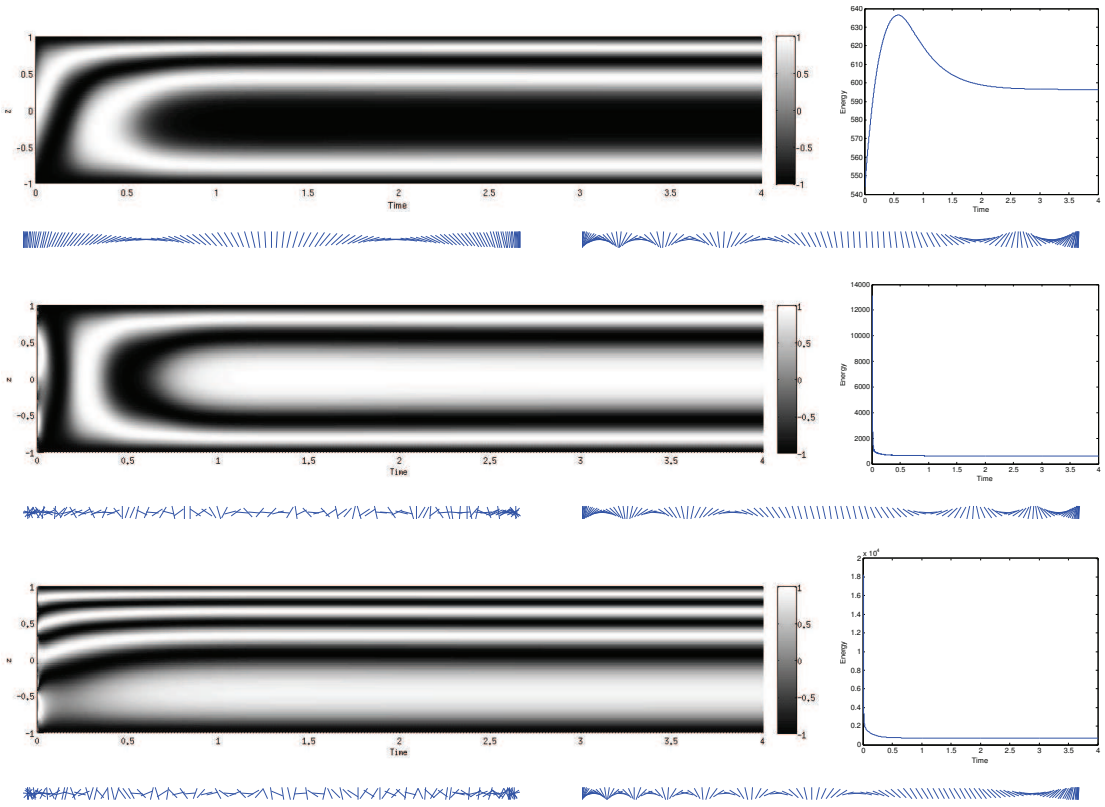

Figure 6: Top: numerical results with initial data in case 1. Notice that due to shear flow the initial configuration is mirror symmetrical while the configuration in steady state is not. Middle: numerical results with initial data in case 2. This example demonstrates the well stability of our numerical method. The configuration goes from disordered state to ordered state rapidly while the total energy decreases quickly. Bottom: numerical results with initial data in case 3.

Now we want to observe the dependency of the solutions on the initial data. Fix $\beta=-0.6$, $\zeta=40$ and $v^0$ as in the above example while change the initial alignments of directors to:

1. $d_2(z)=\cos(\pi z)$, $\quad d_3(z)=\sin(\pi z)$, $\quad z\in[-1,1]$;
2. $A_{init}(z)=2\pi\cdot rand(0,1)$, $\quad d_2(z)=\cos(A_{init}(z))$, $\quad d_3(z)=\sin(A_{init}(z))$, $\quad z\in(-1,1)$, $d_2(-1)=-1$, $\quad d_2(1)=-1$, $\quad d_3(-1)=0$, $\quad d_3(1)=0$;
3. The same as in Case 2,

where $rand(0,1)$ is the function generating random numbers from interval $[0,1]$. The results with these initial values are illustrated in Fig. 6. These examples reveal that the solutions of steady state are not unique and depend on the initial data. We can see the comparison of the alignments in steady states.

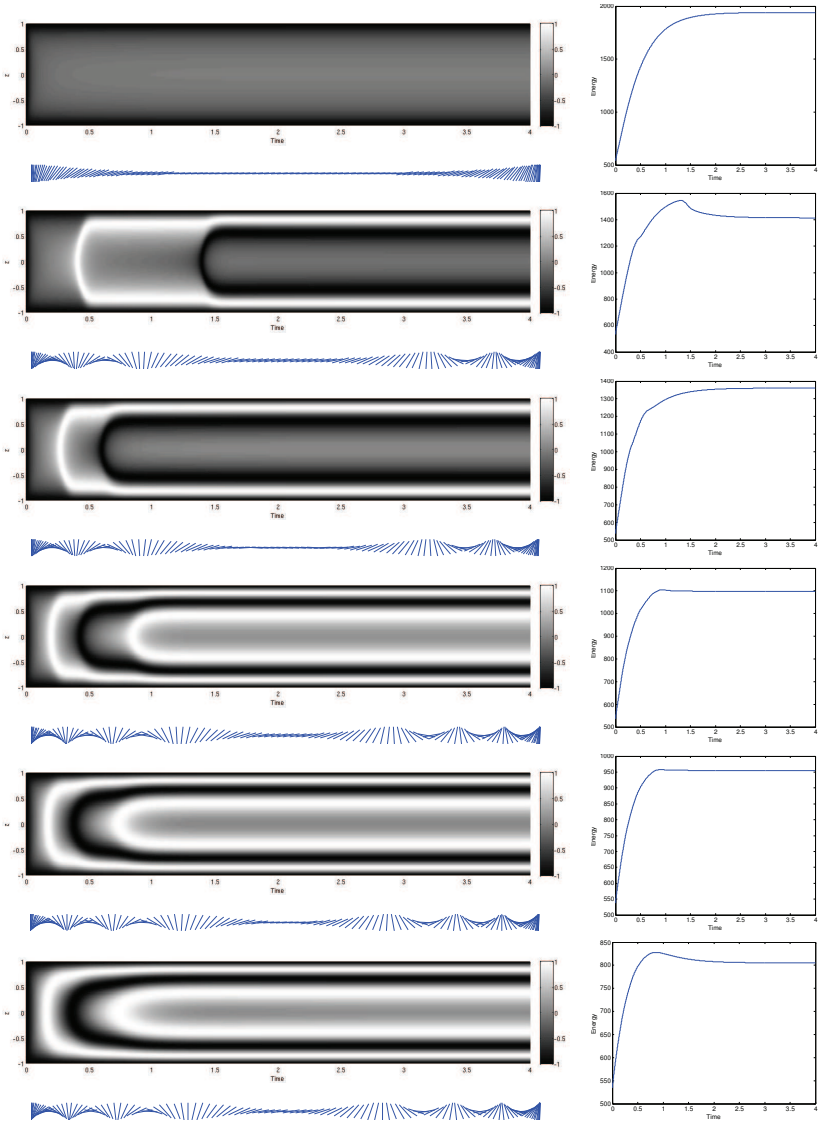

Figure 7: Solutions with different $\beta$. From top to bottom: $\beta=-0.01,-0.05,-0.1,-0.2,-0.3,-0.4$. Below each gray picture is the director configuration at steady state. The figures in the right column are also Energy vs Time.

### 4.3 Shape of molecules

In this subsection we consider the solutions with different $\beta$. First set $\zeta=40$ and $v^0(z)=\zeta z$, $z\in[-1,1]$. We compute solutions with $\beta=-0.01,-0.05,-0.1,-0.2,-0.3,-0.4,-0.5,-0.6,-0.7,-0.8,-0.9,-0.95,-0.99$. The results are depicted in Figs. 7 and 8. In all the simulations the systems go to steady states finally, and the alignments in steady states depend on $\beta$.

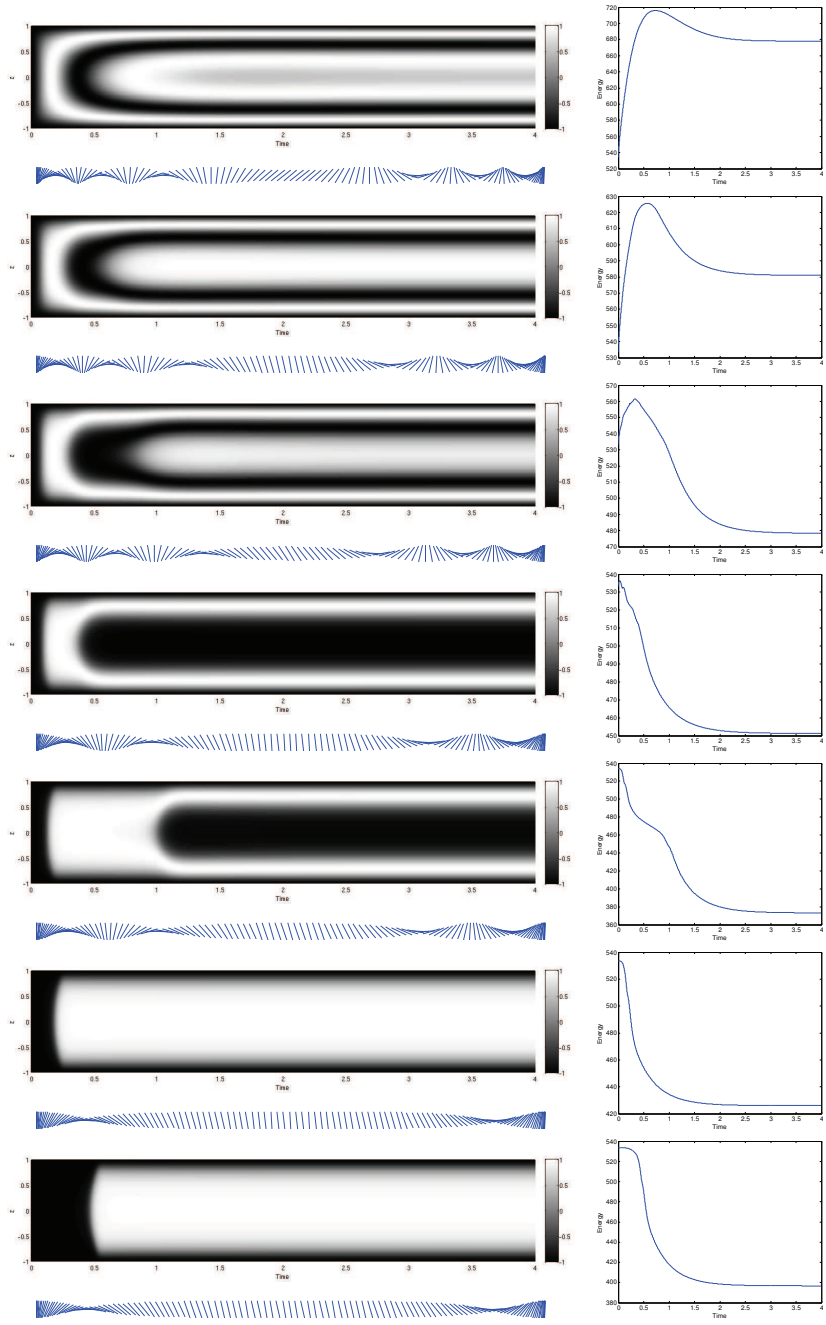

Figure 8: Solutions with different $\beta$. From top to bottom: $\beta=-0.5,-0.6,-0.7,-0.8,-0.9,-0.95,-0.99$.

For our "1+2" model we have

$$D_\beta(\mathbf{u})=\begin{pmatrix} 0 & 0 & 0 \\ 0 & 0 & \beta v_z \\ 0 & (\beta+1)v_z & 0 \end{pmatrix}.$$

When the molecules are rod-like, $D_\beta(\mathbf{u})\cdot(0,1,0)^T = D_{-1}(\mathbf{u})\cdot(0,1,0)^T = \vec{0}$. Similarly, when the molecules are disk-like, $D_\beta(\mathbf{u})\cdot(0,0,1)^T = D_0(\mathbf{u})\cdot(0,0,1)^T = \vec{0}$. Otherwise, $D_\beta(\mathbf{u})\cdot(0,d_2,d_3)^T \neq \vec{0}$ for any $d_2^2+d_3^2=1$ and $v_z \neq 0$. These facts tell us that with proper boundary conditions $d_2, d_3$ have constant solutions for steady states when $\beta=-1$ or $\beta=0$. In other words, all the molecules can stay at the same direction when $\beta=-1$ or $\beta=0$. But when $-1<\beta<0$, it can be checked that constant functions $d_2=c_2$, $d_3=c_3$ with $c_2^2+c_3^2=1$ are not solutions to the steady states.

We can see from Figs. 7 and 8 that when $\beta=-0.01$ and $\beta=-0.99$, which approximate 0 and $-1$, the solutions at steady states approach constant functions. Let $\theta$ be the angle between the director and $y$-axis with $\theta\in[0,2\pi)$ and $\Theta$ be the total change of $\theta$ at steady state defined as

$$\Theta=\int_{-1}^{1}|\theta_z|\mathrm{dz}.$$

We can see from the director alignments at steady states that $\Theta$ attains maximum at $\beta=-0.5$. We give some explanations about this fact. Simply take $d_{2t}=d_{3t}=0$, $d_2^2+d_3^2=1$, $v_z=\zeta$ and consider the following equations:

$$C\beta d_3 = d_{2zz}, \qquad C(\beta+1)d_2 = d_{3zz},$$

where $C=\zeta/\gamma$ is a constant. Let $C_1=\sqrt[4]{-C^2\beta(\beta+1)}/\sqrt{2}$, then $d_3$ has the following four general solutions:

$$\exp(C_1z)\cos(C_1z),\quad \exp(C_1z)\sin(C_1z),\quad \exp(-C_1z)\cos(C_1z),\quad \exp(-C_1z)\sin(C_1z),$$

and the same general solutions for $d_2$. Obviously $C_1$ has maximum value when $\beta=-0.5$. Combined with the properties of sine and cosine function we can see that the fact mentioned above is reasonable. Intuitively, when $\beta=-0.5$ the molecules are spheres. They are easier to rotate than rods, disks and molecules of other shapes.

We want to point out that the total energy increases all the time when $\beta=-0.01$ while in the case $\beta=-0.99$ it decreases. The situation is more complex when $\beta$ is away from 0 and $-1$.

### 4.4 Shear rate

Now we turn to experiments with different $\zeta$. Fix $\beta=-0.6$.

First we compute the solutions when $\zeta=10,20,30,40,50,60$. The results are illustrated in Fig. 9. We can see that the alignments in steady states depend on $\zeta$. The behaviors of the total energy are almost the same in all the cases. It is easy to find that $\Theta$ increases with $\zeta$. This can also be explained by the method we used in the above subsection. Just notice the relationship between $\zeta$ and the general solutions of $d_2$ and $d_3$. Similar phenomenon was observed by Chonoa et al. in [5] where they used a more complicated full EL model.

If we keep on increasing $\zeta$ some periodic solutions can be found, see Fig. 10. In these cases the orientations of most molecules demonstrate a tumbling behavior in the flow

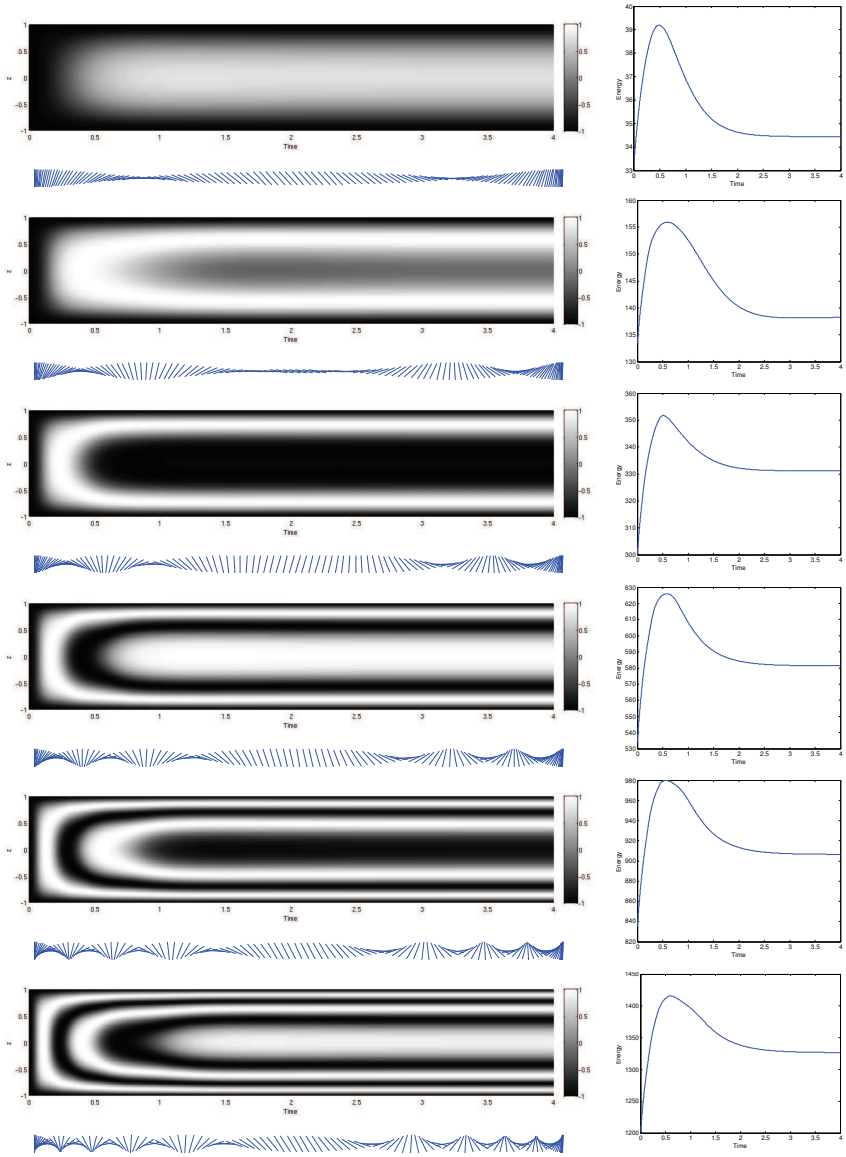

Figure 9: Solutions with different $\zeta$. From top to bottom: $\zeta=10,20,30,40,50,60$. All the solutions go to steady state.

field. It can be seen that singularities appear near the boundary. The fixed boundary and the tumbling region are connected by a thin oscillatory layer. This is reported in [1, 2] as in-plane tumbling-wagging composite state. It includes the competition between the shear stress and the anchoring force. When $\zeta$ is small, the shear stress can not surpass the strength of anchoring, so we just have steady solutions. This situation will change when $\zeta$ is increased.

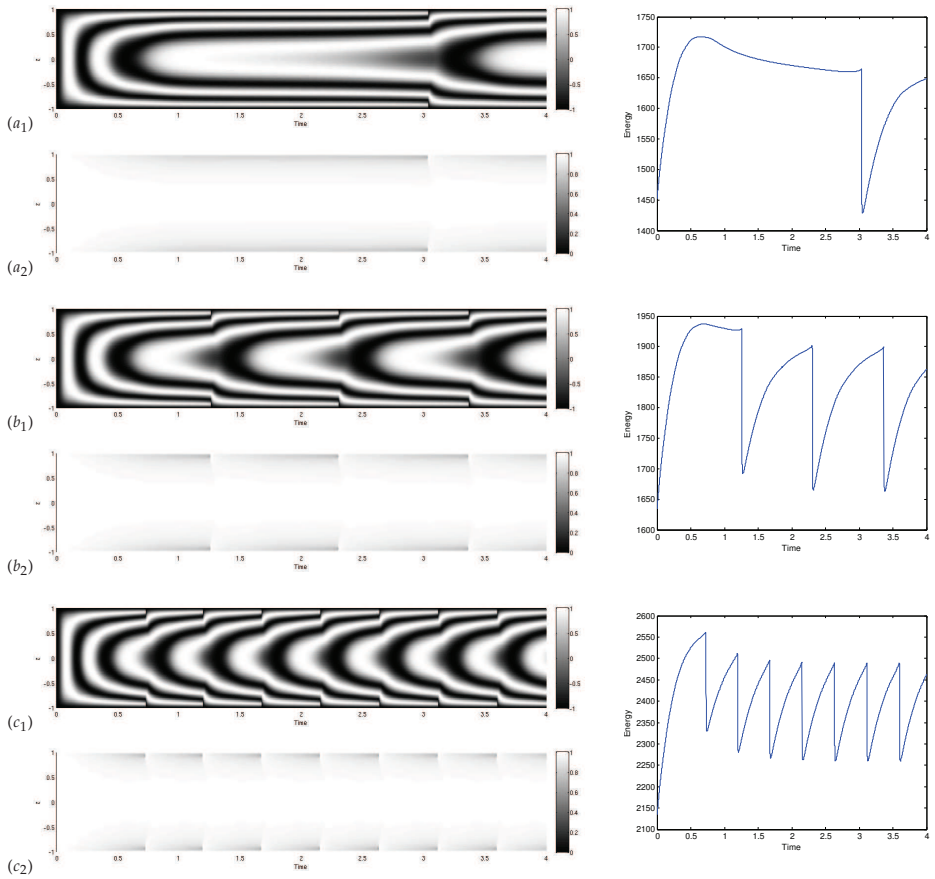


Figure 10: Solutions with different $\zeta$. In $(a_1)(b_1)(c_1)$ the gray colors represent the value of $d_2$. In $(a_2)(b_2)(c_2)$ the gray colors represent the length of the directors. $(a_1)(a_2)$: $\zeta=66$; $(b_1)(b_2)$: $\zeta=70$; $(c_1)(c_2)$: $\zeta=80$. The right column from top to bottom: $\zeta=66$, $\zeta=70$, $\zeta=80$. Periodic solutions are obtained in these cases.

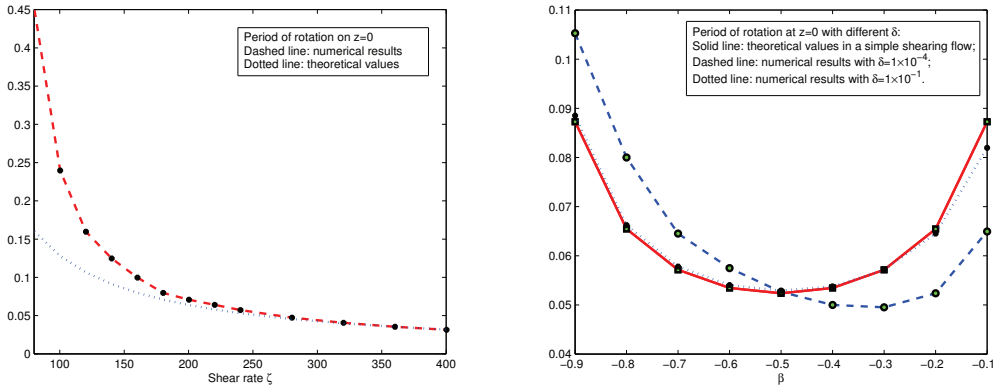


Figure 11: Left: dependence of $P$ on $\zeta$; Right: dependence of $P$ on $\beta$.

Theoretically, the dependence of the tumbling period $P$ on $\zeta$ and $\beta$ is given by [17]

$$P=\frac{2\pi}{\zeta\sqrt{1-(2\beta+1)^2}}. \tag{4.1}$$

This formula can be verified by our simulations. First we can see the dependence of $P$ on $\zeta$ in Fig. 11(left) when $\beta=-0.6$. When $\zeta$ is small, the numerical values do not coincide with the theoretical ones for the effect of the boundary anchoring. But as we increase the value of $\zeta$ they are getting closer.

Set $\zeta=240$, the dependence of $P$ on $\beta$ is depicted in Fig. 11(right). With the strong anchoring $\delta=1\times10^{-4}$ the numerical values differ from the theoretical ones while they are close with the weak anchoring $\delta=1\times10^{-1}$.

### 4.5 Flow-aligning nematic LCs

For flow-aligning nematic LCs with $\beta<-1$ or $\beta>0$, it is predicted by Ericksen-Leslie theory that there are always steady-state solutions and the director orientation is given by [17]

$$\theta=\arctan\left[\pm\left(\frac{\beta+1}{\beta}\right)^{\frac{1}{2}}\right]. \tag{4.2}$$

We list our numerical results for flow-aligning nematic LCs in Tables 1 and 2. The parameters are $\mu=10$ and $\zeta=240$ and the numerical director orientations are taken on $z=0$ at time $t=1$. We can see from the tables that the numerical values are almost the same with the theoretical ones, except when $\beta=0$. This is also due to the strong boundary anchoring. We want to point out that in these simulations a larger $\mu$ is used to insure the convergence of fixed point iteration method.

Table 1: Flow-alignment angle when $\beta<-1$.

| $\beta$ | $-3$ | $-2.5$ | $-2$ | $-1.5$ | $-1$ |
|---|---|---|---|---|---|
| Theoretical (*deg*) | 39.232 | 37.761 | 35.264 | 30.000 | 0.000 |
| Numerical (*deg*) | 39.232 | 37.761 | 35.264 | 30.000 | 0.000 |

Table 2: Flow-alignment angle when $\beta>0$.

| $\beta$ | 0 | 0.5 | 1 | 1.5 | 2 |
|---|---|---|---|---|---|
| Theoretical (*deg*) | $-90.000$ | $-60.000$ | $-54.736$ | $-52.239$ | $-50.768$ |
| Numerical (*deg*) | $-88.539$ | $-60.000$ | $-54.736$ | $-52.239$ | $-50.768$ |

**Remark 4.2.** It is well-known that in simple shear flow, the nematic liquid crystal has another important motion: wagging [1, 2]. The wagging state is not observed in our simulations. We believe that this is due to the lack of short range order elasticity in this model.

**Remark 4.3.** In most of these simulations, the background flow can keep the profile of shear flow very well including the large shear rate cases. The exception is that the background flow has small perturbations near the singularities when the solution is periodic. This conclusion does not depend on $\mu$ heavily.

## 5 Conclusions

We applied the "1+2" elastic continuum model to investigate the effect of kinematic transports. An accurate and efficient Legendre-Galerkin method which can preserve energy law in discrete form was designed. With this numerical method we simulated the behaviors of systems with different kinematic transports. We did some tests of the numerical scheme and gave a criterion to ensure the convergence of fixed point iteration method. Numerical experiments with different $\beta$ and $\zeta$ were carried out. For the systems with steady state solutions, the number of spatial rotations is determined by $\beta$ and $\zeta$, i.e., the shape of molecules and the shear rate. Theoretical analysis was made to explain the results. For the tumbling flow we verified the relationship between the tumbling period and two important parameters. Flow-aligning nematic LCs were also studies by our simulations.

## Acknowledgments

Shupeng Zhang is partially supported by NSF of China 10871028. Chun Liu is partially supported by NSF Grants. Hui Zhang is partially supported by NSF of China 10871028 and state key basic research project of China 2005CB321704.

### References

[1] H. Yu and P. Zhang, A kinetic-hydrodynamic simulation of microstructure of liquid crystal polymers in plane shear flow, J. Non-Newtonian. Fluid. Mech., 141 (2007), 116–227.
[2] T. Tsuji and A. D. Rey, Orientation mode selection mechanisms for sheared nematic liquid crystalline materials, Phys. Rev. E., 57(5) (1998), 5610–5625.
[3] J. J. Feng, J. Tao and L. G. Leal, Roll cells and disclinations in sheared nematic polymers, J. Fluid. Mech., 449 (2001), 179–200.
[4] Q. Wang, A hydrodynamic theory for solutions of nonhomogeneous nematic liquid crystalline polymers of different configurations, J. Chem. Phys., 116(20) (2002), 9120–9136.
[5] S. Chonoa, T. Tsujia and M. M. Denn, Spatial development of director orientation of tumbling nematic liquid crystals in pressure-driven channel flow, J. Non-Newtonian. Fluid. Mech., 79 (1998), 515–527.
[6] F. H. Lin and C. Liu, Existence of solutions for the Ericksen-Leslie system, Arch. Rat. Mech. Anal., 154(2) (2000), 135–156.
[7] F. H. Lin and C. Liu, Nonparabolic dissipative systems modeling the flow of liquid crystals, Commun. Pure. Appl. Math., 48(5) (1995), 501–537.

[8] P. Lin, C. Liu and H. Zhang, An energy law preserving $C^0$ finite element scheme for simulating the kinematic effects in liquid crystal dynamics, J. Comput. Phys., 227(2) (2007), 1411–1427.
[9] C. Liu, J. Shen and X. F. Yang, Dynamics of defect motion in nematic liquid crystal flow: modeling and numerical simulation, Commun. Comput. Phys., 2 (2007), 1184–1198.
[10] C. Liu and N. J. Walkington, Approximation of liquid crystal flows, SIAM J. Numer. Anal., 37(3) (2007), 725–741.
[11] C. Liu and N. J. Walkington, Mixed methods for the approximation of liquid crystal flows, M2AN, 36(2) (2002), 205–222.
[12] P. Lin and C. Liu, Simulations of singularity dynamics in liquid crystal flows: a $C^0$ finite element approach, J. Comput. Phys., 215(1) (2006), 348–362.
[13] Q. Du, B. Y. Guo and J. Shen, Fourier spectral approximation to a dissipative system modeling the flow of liquid crystals, SIAM J. Numer. Anal., 39(3) (2001), 735–762.
[14] H. Zhang and Q. Bai, Numerical investigation of tumbling phenomena based on a macroscopic model for hydrodynamic nematic liquid crystals, Commun. Comput. Phys., 7(2) (2010), 317–332.
[15] P. G. de Gennes and J. Prost, The Physics of Liquid Crystals, Second Edition, Oxford Science, 1993.
[16] J. L. Ericksen, Conservation laws for liquid crystals, Trans. Soc. Rheol., 5(1) (1961), 23–34.
[17] R. G. Larson, The Structure and Rheology of Complex Fluids, Oxford Unversity Press, 1999.
[18] L. A. Archer and R. G. Larson, A molecular theory of flow alignment and tumbling in sheared nematic liquid crystals, J. Chem. Phys., 103 (1995), 3108–3111.
[19] H. Sun and C. Liu, On energetic variational approaches in modelling the nematic liquid crystal flows, Discrete. Cont. Dyn. S., 23 (2009), 455–475.
[20] C. Liu and J. Shen, On liquid crystal flows with free-slip boundary conditions, Discrete. Cont. Dyn. S., 71 (2001), 307–318.
[21] J. Shen and T. Tang, Spectral and High-Order Methods with Applications, Science Press, 2006.